MODELING THE HEAT TRANSFER WHEN A CHEMICALLY REACTING FLOW PASSES A RIB BY MEANS OF THE FINITE-ELEMENT METHOD

A. A. Mikhalevich and V. I. Nikolaev

UDC 536.24:532.54

The finite-element method is used to solve the conjugate problem of heat transfer between a ribbed wall and a chemically reacting flow. The distribution of the velocities, temperatures, and concentrations, as well as the local heat-transfer coefficients and efficiency of the rib, is obtained.

Ribbing heat-transfer surfaces is one of the most widespread and effective methods of intensifying heat transfer. As shown by investigation [1], the distribution of the thermohydraulic parameters in the flow around longitudinally ribbed tube bundles is complex. The temperature difference in the cross section of such bundles may reach several thousand degrees in the initial section.

Increasing the efficiency of ribbing in order to reduce the mass and size characteristics of the ribbed surfaces is an urgent and practically important problem. At present, there are various methods and technologies for the production of ribbed surfaces. In one, a U-shaped groove is welded to the outer surface of a tube in order to produce longitudinal ribbing. The deficiency here is the presence of a technological gap between the base of the groove and the tube surface and the consequent formation of additional thermal resistance.

In engineering practice, the calculation of heat transfer in the rib (and the design of the ribbing) is usually reduced to solving a conductive problem, whereas the complex phenomena of convective heat transfer and hydrodynamics are rarely studied. The influence of convection in this approach to the theory of heat transfer of the rib is taken into account by means of the concept of the heat-transfer coefficient, which is usually taken to be constant over the rib height. It is known that this approach often disagrees with the reality. In addition, the heat-transfer coefficients used in the rib calculation are often determined from approximate estimates.

The investigation of rib heat transfer in the presence of a gap is thus one of the aims of the present work. Since it is impossible to measure experimentally both the temperature drop in the gap and its distribution over the rib height, numerical modeling on a computer is used, on the basis of solution of a system of conservation equations by means of the finite-element method (FEM).

Mathematical Model. Initial Equations

A flow of chemically reacting gas in which the following reactions occur is considered: 1) $N_2O_4 = 2NO_2$; 2) $2NO_2 = 2NO + O_2$; 3) $NO_3 = NO_2 = 0$. The first and third reactions occur in equilibrium, and the second as a reaction occurring at a finite rate [2]. A diagram of the flow and the channel studied is given in Fig. 1.

The transport equations and boundary conditions are written in the following approximation: parabolic flow of Newtonian liquid is considered; leakage of heat along the channel axis is neglected, together with thermodiffusion and barodiffusion; and only the longitudinal component of the velocity vector is taken into account. In this case, the initial system of equations takes the form

$$\rho U \frac{\partial U}{\partial z} = \nabla_{xy} (\mu \nabla_{xy} U) - \frac{\partial \rho}{\partial z}; \quad (1)$$

$$\rho c_p U \frac{\partial T}{\partial z} = \nabla_{xy} (\lambda \nabla_{xy} T) + S_T; \quad (2)$$

Institute of Nuclear Power, Academy of Sciences of the Belorussian SSR, Minsk. Translated from Inzhenerno-Fizicheskii Zhurnal, Vol. 55, No. 2, pp. 202-208, August, 1988. Original article submitted April 23, 1987.

0022-0841/88/5502-0849$12.50

$$\rho U \frac{\partial C}{\partial z} = \nabla_{xy}(D\nabla_{xy}C) + R_C. \tag{3}$$

The continuity equation is expediently used in integral form

$$\int_s \rho U ds = \text{const}. \tag{4}$$

Since the problem is solved in a conjugate formulation, the system is complemented by the heat-conduction equation

$$\nabla^2_{xy} T = 0. \tag{5}$$

The region of integration of Eqs. (1)-(4) is shown in Fig. 1 and consists of two subregions: the ribbed wall of the channel and the region of moving gas. The flow is symmetric relative to the lines AD, BC, CD.

Because the expressions and procedures for determining the coefficients μ, λ, C_p, and D_C of the chemically reacting heat carrier N_2O_4–NO are complex and unwieldy, and on the assumption that this is not fundamental to the solution of the initial system, they are not presented here, nor are the algorithms for calculating the source terms S_T and R_C in Eqs. (2) and (3). They are calculated according to the algorithms and procedures in [2, 3].

Solving the parabolic equations corresponding to the given situation requires boundary conditions at all the boundaries of the region and the values of U, T, C at the channel inlet. Uniform profiles of all the functions (U, T, C) are specified at the channel inlet and Neumann conditions at the symmetry lines; at the outer boundary of the supporting wall AB, provision is made for use of thermal boundary conditions of the first, second, and third kinds. Finally, at the wall–gas heat-transfer surface, conservation conditions for the temperature and normal heat flux are satisfied.

The use of FEM and the Galerkin method leads to a system of nodal differential equations, which may be written in matrix form as follows

$$[C]\left\{\frac{d\Phi}{dz}\right\} + [K]\{\Phi\} + \{F\} = 0; \tag{6}$$

$$[C] = \sum_{e=1}^{N} [C]^{(e)} = \sum_{e=1}^{N} \int_{s_1} A[N]^T [N]\, ds; \tag{7}$$

$$[K] = \sum_{e=1}^{N} [K]^{(e)} = \sum_{e=1}^{N} \int_{s_i} [B]^T [D][B]\, ds; \quad i = 1, 2; \tag{8}$$

$$\{F\} = \sum_{e=1}^{N} \{F\}^{(e)} = \sum_{e=1}^{N} \int_{s} \Theta[N]^T ds + \int_{L_1} q[N]^T dL. \tag{9}$$

For each element of the region, integration and summation over all the elements is undertaken in the usual manner. The values of the quantities appearing in Eqs. (7)-(9) are given in Table 1.

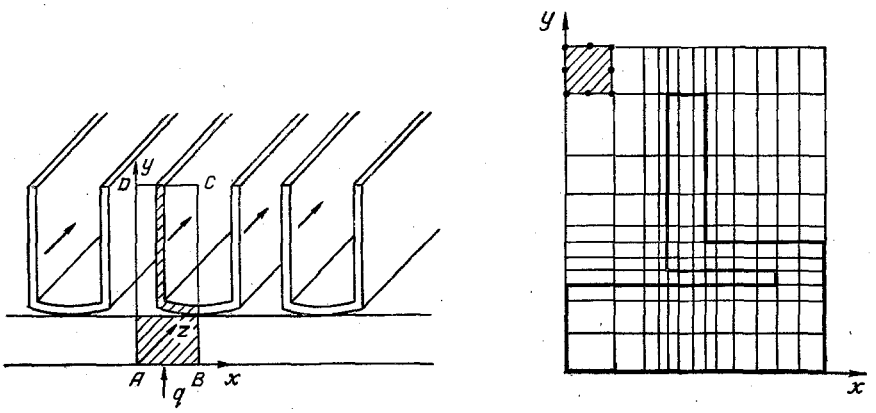

Fig. 1. Diagram of flow and region of integration.

TABLE 1. Values of Coefficients in Eqs. (7)-(9)

Form of equation	A	[D]	0
Motion	U	μ	$-\frac{\partial p}{\partial z}$
Energy	Uc_p	λ_g	0 — inert R_I — chemically reacting
Heat conduction	0	λ_w	0 — no internal heat liberation; q_{int} — internal heat liberation
Diffusion	U	D_4	I_4

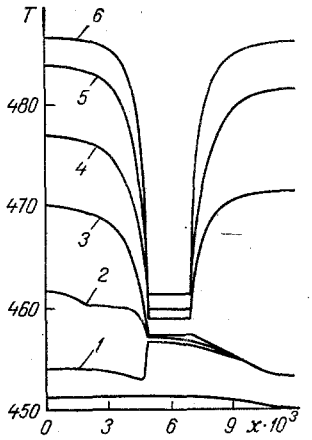

Fig. 2. Distribution of temperature T (x, y = h) with $h \cdot 10^3$ = 5.0 (1), 5.1 (2), 5.3 (3), 6.0 (4), 6.5 (5), and 7.5 (6). T, K; x, m.

Functions of the Lagrangian family for quadratic quadrangles are taken as the basis functions [4]. Integration of the equations downstream is undertaken by a purely implicit two-layer scheme with lead

$$K_{i+1}\Phi_{i+1} + C_{i+1}(\Phi_{i+1} - \Phi_i)/\Delta z - F_{i+1} = 0. \quad (10)$$

The scheme is nonlinear and is solved by an iterative method, as follows

$$[K_{i+1}^{(s)} + C_{i+1}^{(s)}/\Delta z]\,\Phi_{i+1}^{(s+1)} = C_{i+1}^{(s)}\Phi_i/\Delta z + F_{i+1}^{(s)}. \quad (11)$$

Although the algorithm is stable, oscillations may arise in the numerical values of the desired quantity. The amplitude of the oscillations depends on the material, the dimensions of the elements, and the step Δz. Simultaneous decrease in the size of the elements and Δz significantly reduces the amplitude of the oscillations. In solving the system of algebraic equations, the direct Gaussian method is used. The matrices are transformed to strip form. The program has been widely used, without the appearance of any problems associated with convergence or stability of the solution.

Results and Discussion

The program is tested and carefully verified by comparison with experiments and the results of electromodeling, and also by comparing numerical results with analytical calculations.

The temperature distribution in a complex region including the rib, the supporting wall, and the free gas flow is shown in Fig. 2. The initial parameters assumed in the calculation are: T_{in} = 485-685 K; P = 20 bar; $C_{in} = 10^{-1}$-10^{-3}; U_{in} = 0.2-17.5 m/sec; $q_w = 3.5 \cdot 10^3$-0.5×10^6 W/m²; λ_w = 15 W/m·deg. As already noted, the heat carrier chosen is the gas N_2O_4—NO in which chemical reaction is occurring, in this case, with absorption of the heat of dissociation of the N_2O molecules to O_2 and NO. The model also takes account of the influence of excess (in an amount of 3%) content of NO molecules in the heat carrier on the heat and mass transfer. The fundamental qualitative differences between the heat transfer of a chemically

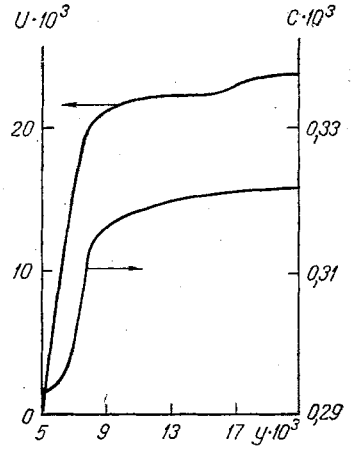

Fig. 3. Distribution of velocity U (x = l, y) and oxygen concentration C (x = l, y) when $l \cdot 10^3 = 3$. U, m/sec; y, m.

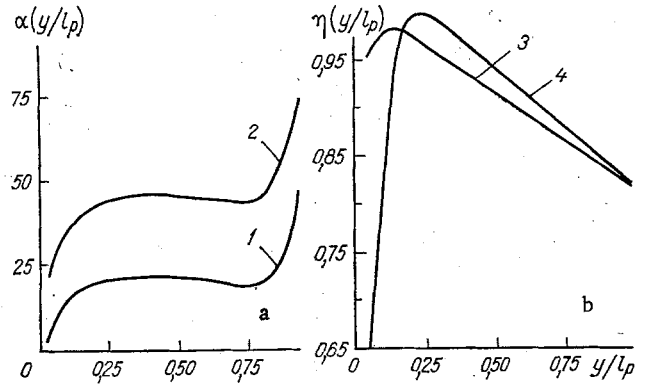

Fig. 4. Distribution of heat-transfer coefficients $\alpha(y/l_p)$ (a) over the rib height for various values of the velocity — U = 0.2 m (1) and 0.8 (2) m/sec — and rib efficiency $\eta(y/l_p)$ (b) over both sides of rib; 3) when $x = 5 \cdot 10^{-3}$, left-hand side in Fig. 5; 4) $x = 7 \cdot 10^{-3}$, right-hand side of rib. α, W/m·deg.

reacting heat carrier and that of an inert medium is that in the first case, as is known, there is additional mass transfer in the transverse direction, and hence also enthalpy transfer on account of the concentrational–diffusion mechanism. This leads to some equalization of the temperature profile in the channel cross section. Temperature redistribution in the supporting wall due to the presence of the ribs and the gap results in redistribution of the heat flux in the supporting wall.

Calculation shows that the distribution of the gas temperature around the rib surface with respect to the normal conforms basically to a parabolic law. A difference is observed in the region adjacent to the base of the rib, where the influence of the supporting wall begins to be felt. The presence of the gap is due to asymmetry in the temperature distribution of the gas to the right and left of the rib. Thus, the difference $\Delta T = T_\infty - T_w$ along Y = 7.5 reachest 25° to the left, while $\Delta T(Y = 7.5) \approx 15°$ to the right of the rib.

The thermal and hydrodynamic boundary layer around the rib amounts to 3-3.5 mm (Figs. 2 and 3), which is in complete agreement with calculations according to the approximate dependence $l/\delta \simeq 1\sqrt{\mathrm{Re}}$.

As would be expected, the intensity of rib operation is not constant over the height, but is a minimum where the velocity of the surrounding flow is a maximum. Admittedly, there are two competing processes for the chemically reacting flow in this case: more intensive heat transfer in the zones of higher velocity; and "freezing" of the flow in these zones. It is evident from the distribution of the heat-transfer coefficients at the rib surface in Fig. 4a that α at the rib vertex is almost four times higher than at the base. The extent of the

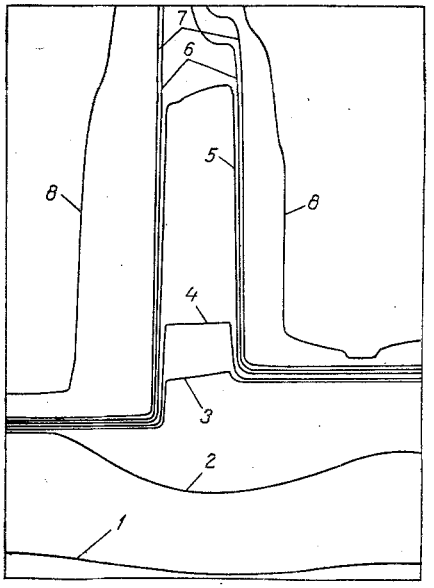

Fig. 5. General picture of isotherms in the given region: 1) 480 K; 2) 490; 3) 520; 4) 540; 5) 590; 6) 620; 7) 650; 8) 680.

zone where the heat-transfer coefficient remains unchanged depends on the velocity of the incoming flow, and is 30-70% of the whole rib surface. It is evident that, with increase in flow velocity, the zone of so-called stable heat transfer decreases. It is clear that extreme caution is required in specifying any mean values of the heat-transfer coefficients at the rib surface in calculating the heat transfer of the ribbed surfaces.

Efficiency of Rib

The basic working characteristics of the rib — the efficiency in engineering practice — is calculated from the well-known dependence

$$\eta = \frac{th(ml)}{ml}, \tag{12}$$

which is obtained from the conductive theory of rib heat transfer. Using the model of conjugate heat transfer between the ribbed wall and the gas flow allows this important characteristic to be calculated directly from the dependence

$$\eta = \frac{q}{q_{ideal}}, \tag{13}$$

where q_{ideal} is the heat-flux density when $\lambda_p = \infty$.

In order to use the latter dependence, the temperature fields over the whole region (including the rib and the flow) are calculated, and the specific heat fluxes are determined with the real value of λ_p and q_{ideal} as $\lambda_p \to \infty$.

The corresponding point values of the rib efficiency are determined using the local values of the specific heat flux q_{loc} at the points located at the sides of the rib calculated respectively when λ = fin and $\lambda \to \infty$, and the dependence $\eta = \eta(y/h_p)$ is plotted. Calculation shows (Fig. 4b) that the maximum value η_{max} is attained not at the base but rather at a distance $(0.15\text{-}0.2)y/h_p$ from the base. The minimum in the distribution of q over the rib height, which corresponds to a corner point at the base of the rib, is associated with local reduction in rib efficiency in the base zone and upward shift of the maximum of $\eta(y)$ over the rib height. The shift in the maximum of the distribution of q and η is due to the specifics of heat transfer at the lower corner point (in the rib base), where there is a local "trough" in the distribution of q at the surface.

In the general case, the temperature difference is a function of the heat-flux density through the gap, and depends on the thermal conditions of operation of the apparatus where the ribbing is used. In nuclear power stations, where the heat-flux density reaches considerable values, disregarding effects associated with the presence of the gaps may lead to

TABLE 2. Temperature Differences in the Gap and Over the Height of the Rib

z/d_G	U, m/sec	q, W/m²	l_p, mm	δ_s, mm	ΔT_s, K	ΔT_p, K
0,25	0,2	$3,5\cdot10^3$	12	0,1	4,0	3,1
0,5					4,5	3,9
40,0					3,4	5,4
100,0					2,6	4,8
136,0					2,4	4,4
0,25	0,2	$3,5\cdot10^3$	12	0,5	4,8	1,5
0,75					6,0	2,5
32,0					5,3	4,0
130,0					4,5	3,7
160,0					4,0	3,5
0.25	17,5	$5\cdot10^5$	12	0,1	8.6	124.0

significant errors. Thus, the theoretical temperature difference ΔT_G with a gap thickness of 0.1 mm, heat-flux density $q_{AB} \approx 3000$-4000 W/m², and $U_{in} = 0.2$ m/sec is 0.5-4.5 K. When $q_{AB} \approx 0.5\cdot10^6$ W/m² and $U_{in} = 17.5$ m/sec, this difference reaches 8-10 K. The temperature gradient in the gap $\Delta T/\delta_G$ reaches $(0.8\text{-}1.0)\cdot10^5$ deg/m. The temperature difference in the gap and the temperature difference over the height of the rib are shown in Table 2.

The composition of the chemically reacting heat carrier is calculated on the basis of solving the diffusion equation for oxygen, the component appearing in all the reactions. The concentration distribution of the components in various zones of the channel allows judgements to be made regarding the intensity of the chemical process (in this case, the molecular dissociation $2NO_2 = 2NO + O_2$). Note that the absolute value of the change $\Delta C = C_\infty - C_w$ is no more than 1% (in the case here considered), while the gradient dC/dx is 10-15 m^{-1}.

A general picture of the temperature distribution over the whole region is shown in Fig. 5. The region of compression of the isotherms corresponds to the greatest temperature gradient in the channel.

Thus, investigation on the basis of numerical modeling allows practically complete information to be obtained on the heat transfer in complex channels, which is especially valuable in cases where experimental investigation is difficult or completely impossible. FEM is especially effective in solving conjugate heat-transfer problems in channels of complex geometry. The bundle of programs based on FEM permits the calculation of local values of the given functions and the analysis of information using a bundle of service programs for various flows (laminar, turbulent) in channels of complex geometry (ribbed tube bundles, rectangular, annular, etc.). The distribution of the heat-transfer coefficients is significantly nonuniform over the rib height. The maximum values are achieved at the vertex and the minimum at the base of the rib. The presence of the gap impairs the efficiency of rib operation and increases the temperature difference over the rib height. The presence of ribbing leads to redistribution of the heat flux in the supporting wall.

Note, in conclusion, that the calculations are performed on an EC-1061 computer requiring 120-150-sec processor time for a single "time" layer. The region is discretized using 200-240 quadratic quadrangles.

NOTATION

U, velocity; T, temperature; C, oxygen concentration; P, pressure; μ, viscosity; c_p, specific heat; λ, thermal conductivity; D, diffusion coefficient; S_T, source (or sink) of thermal energy on account of chemical reactions; R_C, source (or sink) of component on account of chemical reactions; $\nabla_{xy} = \frac{\partial}{\partial x}(\ ) + \frac{\partial}{\partial y}(\ )$; $\nabla^2_{xy} = \frac{\partial^2}{\partial x^2}(\ ) + \frac{\partial^2}{\partial y^2}(\ )$; q, specific heat flux; T_4, source of oxygen components in the chemically reacting flow. Indices: g, gas; w, wall; ∞, in the core of the flow; in, channel inlet; x, y, z, direction of axes in Cartesian coordinate system; $l = 1, N$, summation over all the elements.

LITERATURE CITED

1. A. A. Mikhalevich, V. A. Nemtsev, V. I. Nikolaev, and L. N. Shegidevich, Inzh.-Fiz. Zh., 46, No. 2, 185-189 (1984).

2. V. I. Nikolaev, V. A. Nemtsev, and L. N. Shegidevich, Izv. Akad. Nauk BSSR, Ser. Fiz.-Énerg. Nauk, No. 1, 43-48 (1987).
3. V. B. Nesterenko, Physicochemical and Thermophysical Properties of Chemically Reacting System $N_2O_4 = 2NO_2 = 2NO + O_2$ [in Russian], Minsk (1976).
4. O. Zenkevich, Finite-Element Method in Engineering [in Russian], Moscow (1975).

COMPARISON OF PHYSICAL AND NUMERICAL MODELING OF SUPERSONIC FLOW OVER A CONE

P. A. Voinovich, Yu. P. Golovachev,
I. M. Dement'ev, A. N. Mikhalev,
E. V. Timofeev, and A. A. Fursenko

UDC 519.6:533.6.011.5

Results of a multiapproach study of flow of ideal and viscous gases over conical bodies are evaluated. The experiments were performed with a ballistic device using interferometry.

Interest in the study of supersonic flow over various bodies has been stimulated by this phenomenon's many technological applications. An analytical approach is ineffective because of the significant nonlinearity of the problem and complexity of the flow structures. Initial attempts must involve experiment and numerical methods. Their combined use permits conclusions as to the accuracy and reliability of both measurements and the numerical methods for this class of problems. The present study will compare shock wave contours, gas dynamic function profiles in the shock layer sections, and values of the drag coefficient C_X. A comparison of experimental and calculated values of pressure and thermal flux on the surface of a blunt cone was performed previously [1, 2].

1. The physical experiment was performed with the large ballistic apparatus of the Ioffe Physicotechnical Institute [3]. To obtain optical patterns a diffraction shear interferometer [4] with field of view 200 × 300 mm was used. The light source used was an OGM-20 ruby laser with pulse energy of 0.2 J and pulse length of 30 nsec. Two separate matte scatterers were installed ahead of the condenser in the device illuminator. The laser light was transmitted to the receiver section by a lightguide.

The model of the composite cone (base diameter D = 30 mm) had a velocity V_∞ = 885 m/sec, with Mach number M_∞ = 2.57. The path was filled with air under atmospheric conditions, with Reynolds number as determined by incident flow parameters and diameter of the model base $Re_\infty = 1.12 \cdot 10^6$.

In performing the experiments together with the interferograms direct shadow photographs of the object were obtained in a parallel beam in 10 sections of the device in each of two orthogonal directions. Such a recording of the trajectory allowed measurement of the parameters of model motion and calculation of integral aerodynamic characteristics based thereon [4]. The shadow photographs were also used to determine the position of the head shock wave and the internal waves which develop at the breakpoints of the body directrix. The geometry and centering method chosen insured high stability of the model flight, with attack angle not exceeding 1° over the entire path length. This angle was not considered in the density calculations.

The uncertainty in determining path length difference in the given inhomogeneity did not exceed 0.2-0.3 bands. This value served to establish the statistical dispersion of the density. Using the standard Abel procedure, the distributions of path length difference were used to calculate density profiles in the selected sections.

The drag coefficient C_X was calculated by the method of [5]. For comparison to the resistance coefficient obtained by integration of the calculated pressure and friction forces over the frontal and lateral surface of the model, it is necessary to subtract from C_X the

A. F. Ioffe Physicotechnical Institute, Academy of Sciences of the USSR, Leningrad.
Translated from Inzhenerno-Fizicheskii Zhurnal, Vol. 55, No. 2, pp. 209-212, August, 1988. Original article submitted March 23, 1987.